Journal of Electron Microscopy 60(1): 29–33 (2011)
doi: 10.1093/jmicro/dfq078

Physical: Letter

Calculation of integrated intensities in aberration-corrected *Z*-contrast images

Sergio I. Molina[1,*], Maria P. Guerrero[2], Pedro L. Galindo[2], David L. Sales[1], Maria Varela[3] and Stephen J. Pennycook[3]

[1]Departamento de Ciencia de los Materiales e I.M. y Q.I., Facultad de Ciencias, Universidad de Cádiz, Campus Río San Pedro, s/n, 11510 Puerto Real, Cádiz, Spain, [2]Departamento de Lenguajes y Sistemas Informáticos, CASEM, Universidad de Cádiz, Campus Río San Pedro, s/n, 11510 Puerto Real, Cádiz, Spain and [3]Materials Science and Technology Division, Oak Ridge National Laboratory, Oak Ridge, TN 37831, USA
*To whom correspondence should be addressed. E-mail: sergio.molina@uca.es

Abstract Inclusion of spatial incoherence has been shown to give quantitative agreement between non-aberration-corrected high-angle annular dark-field scanning transmission electron microscopy images and theoretical simulations. Here we show that, using the same approach, a significant improvement in the correlation between calculated and experimental normalized integrated intensities is obtained in the InAsP ternary semiconductor alloy, but residual discrepancies remain. We have demonstrated, in good agreement with experimental intensities obtained in calibrated samples, that normalized integrated intensities show a low dependence on the sample thickness over a wide range of thickness values. This behaviour does not occur in conventional (non-aberration-corrected) images and constitutes a powerful tool for straightforward interpretation of high-resolution images in terms of atomic column-resolved compositional maps.

Keywords *Z*-contrast, HAADF-STEM, high-angle annular dark-field, scanning transmission electron microscopy, aberration-corrected, image simulation

Received 9 February 2010, accepted 21 October 2010, online 24 November 2010

There has been a strong controversy for many years about the reason why a mismatch between experimental and simulated high-resolution electron microscopy images exists, both for phase-contrast and for *Z*-contrast imaging modes. The term *Stobbs factor* has been used to represent the fact that image contrast in experimental phase-contrast high-resolution transmission electron microscopy (HRTEM) images has mostly been found to be markedly less than theory predicts. Recently, however, some significant advances have been made for solving this problem that was established more than one decade ago [1,2]. This historic effect has been proved to result from an underestimate of the instrumental broadening due to the modulation transfer functions of CCD cameras used for digital image acquisition [3]. As for the *Z*-contrast imaging mode [4,5], a lack of quantitative matching has also been found between experimental and simulated images. This fact has usually been expressed in terms of a significant background intensity in experimental *Z*-contrast images [6]. Recently, this apparent lack of fit has been solved in non-aberration-corrected *Z*-contrast images by introducing the influence of spatial incoherence in simulated images [7,8]. However, quantitative matching between experimental and simulated aberration-corrected *Z*-contrast images has not

© The Author 2010. Published by Oxford University Press [on behalf of Japanese Society of Microscopy]. All rights reserved.
For permissions, please e-mail: journals.permissions@oup.com

Downloaded from jmicro.oxfordjournals.org at Universidad de Cadiz on February 9, 2011

been reached up to now. We show in this paper that the inclusion of spatial incoherence in aberration-corrected high-resolution *Z*-contrast images gives an approximate agreement with the experimental data, to within 10%, indicating that additional factors may be involved. We prove the validity of this approach by comparing normalized integrated intensities of simulated images with the intensities experimentally evaluated in samples of calibrated composition [9]. An important difference between corrected and non-corrected *Z*-contrast images is the dependence of normalized intensities on the thickness of the electron-transparent specimen. This dependence is significant for non-corrected images [10], whereas it is very low for a range of specimen thicknesses in aberration-corrected images. Concerning the process of interpretation of high-resolution *Z*-contrast images, which offer simultaneous structural and compositional resolution at atomic column scale, this fact is extremely important, and we have contributed to explain it theoretically. Many efforts have been devoted to improve the quantitative interpretation of the high-resolution Z-contrast technique [11], and our paper therefore provides an important step towards this goal.

We have recently published a phenomenological approach to determine quantitatively the composition of an AB_xC_{1-x} alloy with atomic-column resolution [9]. This method is based on the analysis of normalized integrated intensities (R) of high-resolution aberration-corrected *Z*-contrast images of materials of known composition. The R values are calculated as the quotient of the integrated intensity around the anionic (B_xC_{1-x}) columns of the AB_xC_{1-x} alloy and the integrated intensity around the anionic column (C) of the AC binary compound, which is taken as a reference value. The R values are determined for a range of experimental values of composition (x) and thickness of the electron-transparent specimen (t). The R values are determined from experimental raw *Z*-contrast images for several known values of x and t, for the $InAs_xP_{1-x}$ alloy in reference [9], and are represented in Fig. 1. The images were obtained with a positive offset to avoid clipping artefacts, which was then subtracted to give the proper zero signal level. R depends linearly on x and has a low

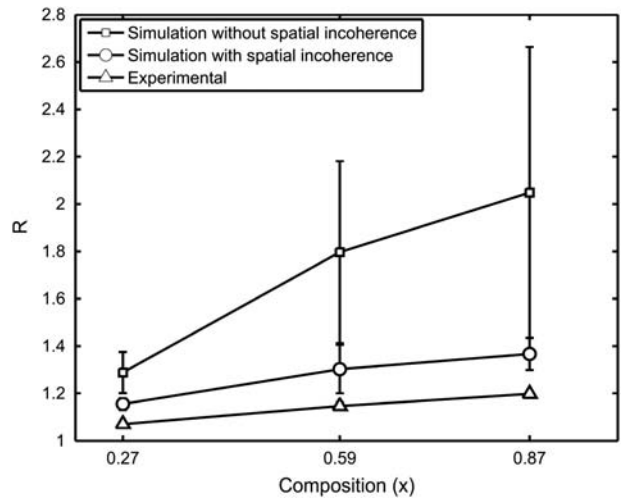

Fig. 1. Experimental and simulated R ratios versus specimen thickness (with and without introducing the effect of spatial incoherence) for three compositions of the $InAs_xP_{1-x}$ alloy. Experimental R data for the whole range of analysed thicknesses is presented in Table 1 of reference [9].

dependence on t (represented in Fig. 1 as error bars of R values) in the range of thickness values used in our experiments (from 16.1 to 40.0 nm). The low dependence of R on t is a very useful result that makes easier the quantitative determination of column-to-column composition in materials from the analysis of high-resolution aberration-corrected *Z*-contrast images. In the following, we explain these experimental results based on dynamical simulations.

All simulation results have been obtained using SICSTEM software [12]. This software runs in the CAI supercomputer at the University of Cadiz (peak performance = 3.75 Tflops), and can afford HAADF-STEM image simulations of nanostructures composed of several hundred thousand atoms in manageable time. Its accuracy has been compared with Ishizuka's FFT multislice approach using the WinHREM™ software, and takes into account thermal diffuse scattering (TDS) in the calculation of the intensity in the object exit plane by the multislice method using a local TDS absorptive potential approach [13,14]. Imaging conditions were chosen to emulate images taken at 100 kV using a dedicated VG Microscopes HB501UX STEM equipped with a Nion aberration corrector. The third- and fifth-order spherical aberration coefficients are (nominally) −50 µm and 63 mm, respectively, the inner detector angle is 64 mrad and the objective

Downloaded from jmicro.oxfordjournals.org at Universidad de Cadiz on February 9, 2011

aperture angle is 27 mrad. Spatial incoherence has been taken into account by applying a convolution with a 2D Gaussian kernel, as suggested previously [7,15,16].

The R ratios calculated by using the explained approach [12] with and without introducing the effect of the spatial incoherence are represented in Fig. 1. For each composition, the R values were calculated in both cases for the specimen thicknesses that were measured by electron energy loss spectroscopy [9]. These thickness values are presented in Table 1 of [9]. The calculated R values, represented in Fig. 1, correspond to the values averaged for the selected range of specimen thicknesses. Error bars correspond to the standard deviation associated with the variation of the R values within this range. As can be seen in Fig. 1, the R values calculated without including the effect of spatial incoherence clearly overestimate the experimental R values. On the contrary, experimental and calculated R values are much closer when a Gaussian is used to take into account the effect of spatial incoherence.

In order to determine the optimum value of the width (standard deviation) of the Gaussian function that gives the best fit between experimental and calculated images, we have considered an error function defined as the sum of squared differences between simulated and experimental Z-contrast images. Figure 2 represents the dependence of these errors on the width of the Gaussian for InP. The minimum value of the error function occurs when the optimum width of the Gaussian function is 0.06 nm, which corresponds to a source size with a full width at half maximum (FWHM) of 0.14 nm. Although this value may seem high, it should be noted that the microscope was operated in a high current mode for energy loss spectroscopy, which would increase the probe size by 0.3–0.4 Å compared with its theoretical optimum size of 0.71 Å FWHM. Furthermore, no explicit account was taken of any non-round or chromatic aberrations which are therefore included as an additional average broadening. The value is consistent with the fact that the dumbbells are not well resolved in $InAs_{0.27}P_{0.73}$, as shown in Fig. 1b of reference [9]. Based on these numbers for the effective source size and the expected aberration-free probe, we obtain a total expected FWHM of 1.57 Å, which is 5.7% larger than the separation of In and As-P columns in this alloy (1.48 Å).

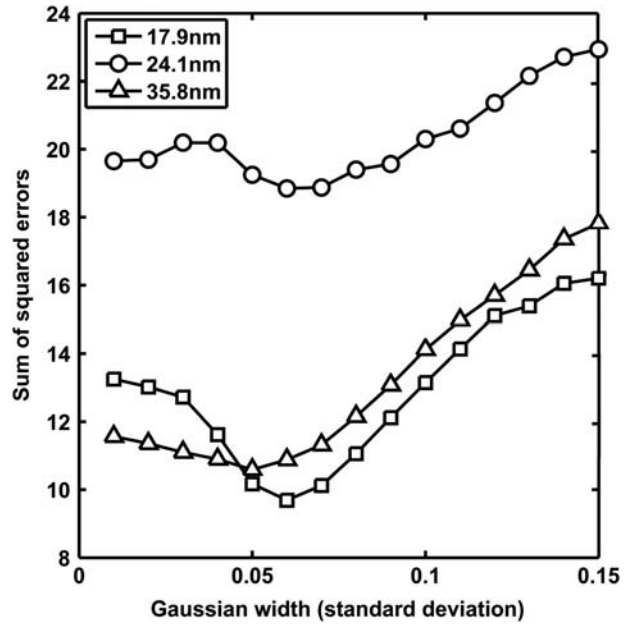

Fig. 2. Sum of squared errors between experimental and simulated Z-contrast images of InP for several specimen thickness as a function of the width of the Gaussian used in order to take into account the effect of spatial incoherence.

For each composition, the R ratios were determined using the optimum value of the source size as the average R values over a thickness range of 16–40 nm. As Fig. 1 shows, a significant improvement in the fitting of experimental and simulated intensities is obtained after introducing the effect of spatial incoherence. Therefore, the assumption that spatial incoherence can be quantified in aberration-corrected HAADF-STEM images by convoluting the coherent simulated images with a two-dimensional Gaussian function is found to be a good one, although a residual error of ~10% remains. It is worth noticing that (i) a unique value of the source size for a range of specimen thickness and composition values is used in our approach, (ii) the small values of the differences among experimental and simulated R ratios and (iii) its small dispersion with the composition and specimen thickness.

An important experimental finding is that, for a certain range of thicknesses, the R values show a very low dependence on the specimen thickness. This is noticeable because with a simple estimation of the specimen thickness, typically in the range of

Downloaded from jmicro.oxfordjournals.org at Universidad de Cadiz on February 9, 2011

15–40 nm for semiconductor ternary alloys, the measurement of R ratios gives atomic column-to-column compositional information. This does not happen for non-aberration-corrected scanning transmission electron microscopes, for which a significant dependence of R on thickness is found [10]. We have also found that the low dependence of R with the specimen thickness also occurs using normalized intensities integrated over the whole projected unit cells, instead of taking a square integration area surrounding the anionic columns (as we did in reference [9]). It is important to note, for the purposes of generalization, that this remains valid for other semiconductor materials. We have calculated the R values using whole projected unit cells as integration areas for two ternary semiconductor alloys ($In_xGa_{1-x}As$ and $GaAs_xSb_{1-x}$), including correction of spherical aberration and the effect of spatial incoherence, for a range of specimen thicknesses, and the R values obtained are represented in Fig. 3 for three compositions. Figure 3 shows how our calculations confirm the low dependence of R with specimen thickness for the two selected semiconductor materials. As we explain in the following paragraph, we think that this is quite likely to be a general behaviour for a wide range of materials.

High-energy electrons travelling along a zone axis tend to channel along atomic columns. We have calculated for an electron probe focussed on the material surface how deep electrons channel in the alloy studied in this work ($InAs_xP_{1-x}$). Figure 4 represents the intensity of the electron wave versus the specimen thickness at the anionic (As-P) projected position, for an electron beam travelling along the [110] zone axis for the $InAs_{0.87}P_{0.13}$ composition, that represents the higher As composition used in our work. This calculation has been done for the experimental imaging conditions of the present work. It can be noticed that electrons channel along [110] in the material from the surface down to ~15–20 nm. All the Z-contrast images analysed in this work, and usually Z-contrast images taken in general by other authors for analytical purposes, are acquired with the electron beam in-focus or close to in-focus condition. Therefore, most of the Z-contrast signal will come from the depth of the material affected

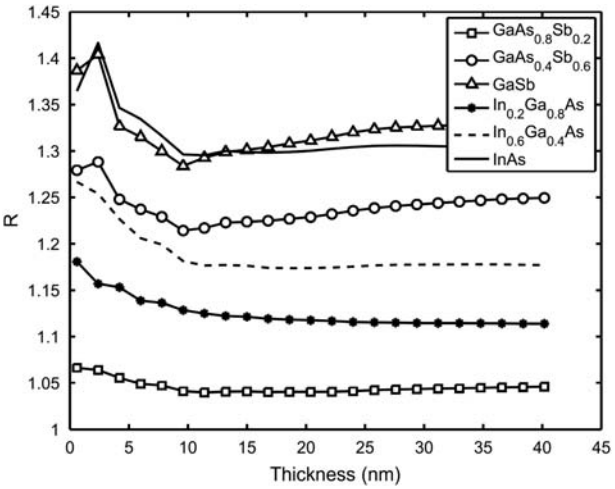

Fig. 3. Simulated R values versus specimen thickness for several compositions of $In_xGa_{1-x}As$ and $GaAs_xSb_{1-x}$ alloys.

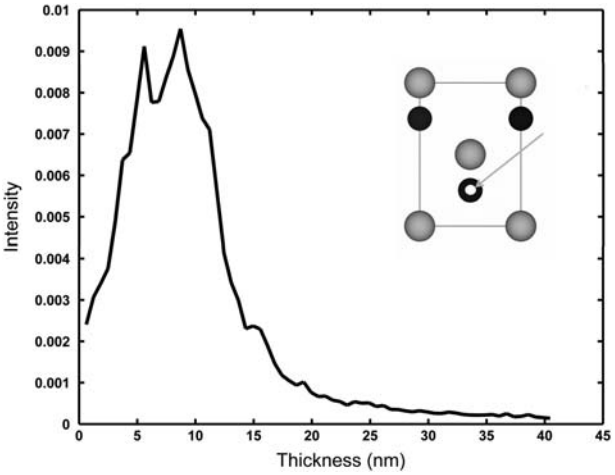

Fig. 4. Intensity at the anionic (As-P) projected position of an electron wave versus the specimen thickness, for an electron beam travelling along the [110] zone axis for $InAs_{0.87}P_{0.13}$, for the imaging conditions used in this work.

by channelling, ~15–20 nm in our case, and more generally of the order of one or few tens of nanometres for many other materials that were studied in the VG501 scanning transmission electron microscope used in our work. These numbers will be smaller for scanning transmission electron microscopes with higher spatial resolution, but the overall picture describing the experiment will be similar. The effect of the electron channelling explains why normalized intensities, expressed in terms of the R ratio, have a very low dependence on the specimen thickness. This makes sense for electron beams focussed using an aberration-corrected lens, because the signal-to-noise ratio is

Downloaded from jmicro.oxfordjournals.org at Universidad de Cadiz on February 9, 2011

very high and electron signal strongly peaks up when the probe is located at atomic columns. This phenomenon will remain valid for specimen thickness below a critical value, ~40 nm in our case, because in thicker specimens electrons will suffer from complex multiple scattering from deeper lying material that will introduce an additional contribution to the *Z*-contrast signal from materials located at thickness below this critical thickness. It is worth pointing out that consideration of the explained effect associated with strong channelling is important in samples with heterogeneous composition along the electron beam path, to avoid erroneous interpretations.

In conclusion, integrated intensities in aberration-corrected high-angle annular dark-field scanning transmission electron microscopy images have been simulated by including the effect of spatial incoherence. By comparison of simulated and experimental images acquired in InAsP thin layers with calibrated compositions, this effect is shown to improve correlation between intensities in both images. A residual error of ~10%, however, cannot be accounted for, and the most obvious origin of this error would be the effect of non-round aberrations that were not recorded when the experimental data were obtained. These non-round aberrations are expected to be quite dependent on the exact tuning of the aberration corrector, and further work is required to determine whether they could quantitatively account for the residual discrepancy. The calculated normalized intensities are found to be almost independent of the specimen thickness in a practical range of useful thickness values, in good agreement with the experimental results, and in contrast with the observed behaviour in non-aberration-corrected images. Based on dynamical simulations of the channeling process that electron beams suffer after propagating along an atomic column, our findings are explained and predicted to be valid for a wide range of materials studied by aberration-corrected *Z*-contrast imaging. Our results pave the way for a direct interpretation of aberration-corrected high-resolution *Z*-contrast images, in terms of elemental compositions with atomic column spatial resolution.

Funding

This work was supported by the Spanish MCI (projects TEC2008-06756-C03-02/TEC and CONSOLIDER INGENIO 2010 CSD2009-00013) and the Junta de Andalucía (PAI research groups TEP-120 and TIC-145; project P08-TEP-03516). Work at ORNL was sponsored by the U.S. Department of Energy, Office of Science, Materials Sciences and Engineering Division (M.V. and S.J.P.).

References

1 Hytch M J and Stobbs W M (1994) Quantitative comparison of high-resolution TEM images with image simulations. *Ultramicroscopy* **53**: 191–203.

2 Howie A (2004) Hunting the Stobbs factor. *Ultramicroscopy* **98**: 73–79.

3 Thust A (2009) High-resolution transmission electron microscopy on an absolute contrast scale. *Phys. Rev. Lett.* **102**: 220801.

4 Pennycook S J and Jesson D E (1990) High-resolution incoherent imaging of crystals. *Phys. Rev. Lett.* **64**: 938–941.

5 Varela M, Lupini A R, van Benthem K, Borisevich A Y, Chisholm M F, Shibata N, Abe E, and Pennycook S J (2005) Materials characterization in the aberration-corrected scanning transmission electron microscope. *Ann. Rev. Mater. Res.* **35**: 539–569.

6 Klenov D O and Stemmer S (2006) Contributions to the contrast in experimental high-angle annular dark-field images. *Ultramicroscopy* **106**: 889–901.

7 LeBeau J M, Findlay S D, Allen L J, and Stemmer S (2008) Quantitative atomic resolution scanning transmission electron microscopy. *Phys. Rev. Lett.* **100**: 206101.

8 LeBeau J M and Stemmer S (2008) Experimental quantification of annular dark-field images in scanning transmission electron microscopy. *Ultramicroscopy* **108**: 1653–1658.

9 Molina S I, Sales D L, Galindo P L, Fuster D, Gonzalez Y, Alen B, Gonzalez L, Varela M, and Pennycook S J (2009) Column-by-column compositional mapping by Z-contrast imaging. *Ultramicroscopy* **109**: 172–176.

10 Grillo V and Carlino E (2008) Influence of the static atomic displacement on atomic resolution Z-contrast imaging. *Phys. Rev. B* **77**: 054103.

11 Robb P D and Craven A J (2008) Column ratio mapping: a processing technique for atomic resolution high-angle annular dark-field (HAADF) images. *Ultramicroscopy* **109**: 61–69.

12 Pizarro J, Galindo P L, Guerrero E, Yáñez A, Guerrero M P, Rosenauer A, Sales D L, and Molina S I (2008) Simulation of high angle annular dark field scanning transmission electron microscopy images of large nanostructures. *Appl. Phys. Lett.* **93**: 153107.

13 Ishizuka K (2002) A practical approach for STEM image simulation based on the FFT multislice method. *Ultramicroscopy* **90**: 71–83.

14 Findlay S D, Allen L J, Oxley M P, and Rossouw C J (2003) Lattice-resolution contrast from a focused coherent electron probe. Part II. *Ultramicroscopy* **96**: 65–81.

15 Dwyer C, Erni R, and Etheridge J (2008) Method to measure spatial coherence of subangstrom electron beams. *Appl. Phys. Lett.* **93**: 021115.

16 Nellist P D and Rodenburg J M (1994) Beyond the conventional information limit—the relevant coherence function. *Ultramicroscopy* **54**: 61–74.

Downloaded from jmicro.oxfordjournals.org at Universidad de Cadiz on February 9, 2011